Synthesis, crystal structure and optical absorption of $NaInS_{2-x}Se_x$

Natsuumi Takahashi[a], Hiroaki Ito [b], Akira Miura[b] *, Nataly Carolina Rosero-Navarro[b], Yosuke Goto[c], Yoshikazu Mizuguchi[c], Chikako Moriyoshi[d], Yoshihiro Kuroiwa[d], Masanori Nagao[a], Satoshi Watauchi[a], Isao Tanaka[a], Kiyoharu Tadanaga[c]

[a] Center for Crystal Science and Technology, University of Yamanashi, 7-32 Miyamae, Kofu, Yamanashi 400-8511, Japan
[b] Faculty of Engineering, Hokkaido University, Kita-13, Nishi-8, Kita-ku, Sapporo, Hokkaido 060-8628, Japan
[c] Department of Electrical and Electronic Engineering, Tokyo Metropolitan University, 1-1 Minami-osawa, Hachioji, Tokyo 192-0397 Japan
[d] Department of Physical Science, Hiroshima University, 1-3-1 Kagamiyama, Higashihiroshima, Hiroshima 739-8526, Japan

* Corresponding Author.
E-mail address: amiura@eng.hokudai.ac.jp (A. Miura)

Keywords:
Solid state reactions
Crystal structure
X-ray diffraction
Synchrotron radiation

Abstract

Although $NaInS_2$ and its isostructural $NaInSe_2$ have been known for more than half a century, these solid solutions have not been investigated. In this work, three layered chalcogenides, $NaInS_{1.5}Se_{0.5}$, NaInSSe, and $NaInS_{0.5}Se_{1.5}$ were synthesized by ball milling and subsequent heating. In-situ synchrotron X-ray diffraction showed that these three chalcogenides were isostructural with $NaInS_2$/$NaInSe_2$ above 550 K, and were stable below 820 K. The mixed occupancy of S and Se were confirmed by Rietveld refinements; the band gap of NaInSSe was estimated to be 2.31 eV by its optical absorption.

1. Introduction

Chalcogenide semiconductors have been actively pursued for decades. The control of their physical properties, such as band gap and transportation properties, are important for many applications, such as photocatalysts and photovoltaics. The tuning of the band structures can be achieved by alloying different chalcogenides [1], changing the dimensions of the crystal structures [2], or decreasing the particle size [3]. A classic example is the CdS-CdSe system, which shows a band-gap range from 2.5 [4] to 1.72 eV [1]. Copper indium gallium selenide (CIGS) is a practical material for photovoltaics [5-7], of which electronic structure can be tuned by alloying with S and Se.

The crystals of $NaInS_2$ [8] and $NaInSe_2$[9], having layered rock salt structures (Fig. 1), have been reported in 1873 and 1961, respectively. The band gap of $NaInS_2$ was experimentally estimated to be 2.3–3.2 eV [10, 11], and that of $NaInSe_2$ was calculated as 2.26 eV by density functional theory using a hybrid functional approach [12]. The band structures and partial density of states (pDOS) of $NaInS_2$ and $NaInSe_2$ have also been calculated by a generalized gradient approximation (GGA) method [13, 14]. These electronic structures are computationally predicted to be of the indirect semiconductors. $NaInS_2$ and $NaInSe_2$ have also received significant attention as unintentional dopants of $CuInS_2$ and $CuInSe_2$. [12, 15, 16] Moreover, $NaInS_2$ is a precursor for many sulfide/oxysulfide photocatalysts and phosphors: $CuInS_2/NaInS_2$,[17] $NaInS_2/MgIn_2S_4$,[16] $CuInS_2/MgIn_2S_4$,[17] $In_2S_3/ZnIn_2S_4$ [18], $PbInS_2$-incorporated $NaInS_2$,[19] and $LaOInS_2$.[20] However, $NaInS_{2-x}Se_x$ solid-solutions have not been investigated. They can be expected to have electronic structures tunable by changing the ratio of S/Se.

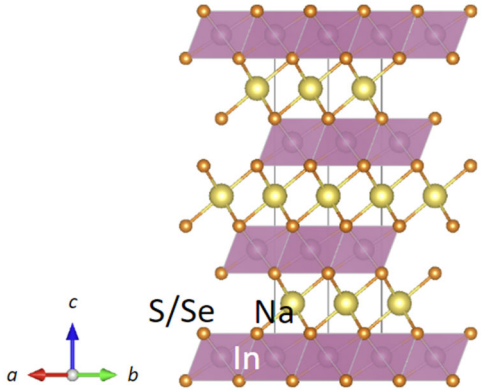

Fig. 1. Crystal Structure of $NaInS_{2-x}Se_x$.

In-situ X-ray diffraction is a useful tool for examining reaction mechanisms, deciding the synthesis or the reaction conditions, and identifying the phase stability. For example, a mechanochemical reaction can be monitored in real time using high-energy synchrotron X-rays.[21] Shoemaker et al. monitored the ternary K-Cu-S and K-Sn-S systems and examined the formation of known and new phases upon heating and cooling.[22] Andrew J. Martinolich et al. studied the reaction mechanism of solid-state metathesis reactions by in-situ XRD, and found that the reaction pathways depended on the exposure to air.[23]

In this study, we successfully synthesized $NaInS_{2-x}Se_x$ (x = 0.5, 1.0, 1.5), isostructural with $NaInS_2$ and $NaInSe_2$, by ball milling and subsequent heating. The heating conditions were determined using in-situ X-ray diffraction. We investigated their crystallization and thermal-stability behavior, as well as their optical absorption.

2. Experimental

$NaInS_{2-x}Se_x$ were synthesized by solid-state reaction in a ball milling process. Na_2S (Aldrich: 97.0-103.0 % from titration by $Na_2S_2O_3$), In_2S_3 (Mitsuwa Chemical: 99.999 %), and In_2Se_3 (Aldrich: 62.9-64.8 % of Bi from gravimetric analysis) were used as starting materials. The powders were mixed with a motor and pestle according to the nominal compositions for $NaInS_{2-x}Se_x$ (x = 0, 0.5, 1.0, 1.5), in an Ar-filled glovebox. One gram of the mixed powder was loaded under argon atmosphere

into a zirconia grinding jar with zirconia balls of 30 g and 4 mm diameter each. The powder was ball-milled for 14 hours at 450 rpm.

Synchrotron XRD was performed at beamline BL02B2 of SPring-8 with a wavelength of 0.49559 Å (proposal No.: 2017B1211). The sample powder was loaded in a quartz capillary with 0.2 mm diameter and sealed under vacuum. The experiments were performed with a sample rotator system at 300–900 K, and the diffraction data were collected using a high-resolution one-dimensional semiconductor detector (multiple MYTHEN system)[24] with a step of $2\theta = 0.006^{o}$. The crystal structure parameters were refined using the Rietveld method with RIETAN-FP [25]. Schematic images of the crystal structure were drawn using VESTA [26]. Energy dispersive X-ray spectroscopy (EDX) was used for the elemental analysis (Hitachi: Miniscope TM3030Plus). The optical absorption was measured by the reflectance spectrum with 1.8–4 eV (JASCO: MSV-5000 series).

First-principle calculations were performed using the Vienna *Ab initio* Simulation Package (VASP)[27]. The projector-augmented wave approach (GGA) [28, 29] and the generalized PBE-type gradient approximation were used [30]. An energy cutoff of 400 eV and rhombohedral cell of $NaInS_2$ and $NaInSe_2$ were used.

3. Results and Discussion

Fig. 2 shows the in-situ XRD patterns of ball-milled $NaInS_xSe_{2-x}$ heated from 300 to 900 K at a rate of 10 K/min. Even without heating, ball-milling-synthesized $NaInS_{1.5}Se_{0.5}$ ($x = 0.5$), showed a low-crystalline phase isostructural with $NaInS_2$. An increase in temperature improved its crystallinity. The crystallinity of $NaInS_{1.5}Se_{0.5}$ suddenly improved at approximately 550 K and the phase of $NaInS_{1.5}Se_{0.5}$ was stable up to 900 K. A similar trend was also observed in NaInSSe ($x = 1$). The low-crystalline NaInSSe phase changed into high-crystalline at approximately 550 K. At a temperature above 850 K it formed peaks which could not be indexed as known phases; these peaks were found in $NaInS_{0.5}Se_{1.5}$ ($x = 1.5$), at high temperature. $NaInS_{0.5}Se_{1.5}$ was synthesized as an amorphous phase after ball milling. There were small peaks which could not be indexed. $NaInS_{0.5}Se_{1.5}$ was formed isostructural with $NaInS_2$/$NaInSe_2$ at 550 K but changed into other peaks above 820 K. The diffraction

peaks at 900 K could not be indexed as a single phase, suggesting its decomposition or the reaction with a quartz capillary. Energy dispersive X-ray spectroscopy detected a Si peak in the position where Na, In, S and Se peaks were also detected. This suggests the reaction with a quartz capillary above 820 K although further investigation is necessary to understand more details in this reaction. Therefore, Se substitution, in the range between $x = 0.5–1.5$, formed isostructural layered rock salt structures by ball milling and a subsequent heating process.

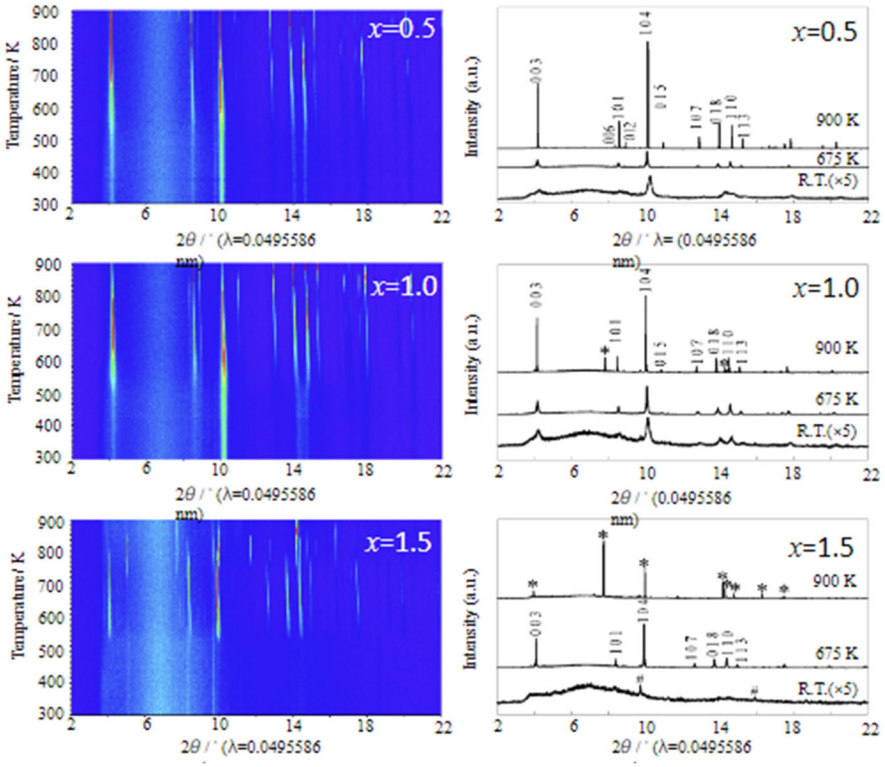

Fig. 2. Synchrotron X-ray diffraction patterns of ball-milled $NaInS_{2-x}Se_x$ heated up to 900 K at a rate of 10 K/min. Left figures are the temperature profiles and the peak intensities, depicted by a gradient from red to blue, in descending order. Right figures are the XRD patterns at 300, 675, and 900 K. The diffraction peaks that could not be indexed are indicated by # and *.

Further characterization (crystal structure and optical absorption analysis) were performed on the products heated at 675 K, which crystallized in a layered rock salt structure, isostructural with $NaInS_2$/$NaInSe_2$. No structural transition occurred when cooling from 675 to 300 K. Fig. 3 shows the Rietveld profile of the synchrotron

X-ray diffraction measured at 300 K. The refinements were performed with a hexagonal cell with space group $R\bar{3}m$, and isostructural with $NaInS_2$/$NaInSe_2$. The lattice parameters of $NaInS_{2-x}Se_x$ with x = 0.5-1.5 at 300 and 675 K are summarized in Fig. 4. They increase almost linearly with increasing Se content, x, and are larger at 650 than at 300 K. Refinements and structural factors are summarized in Table 1.

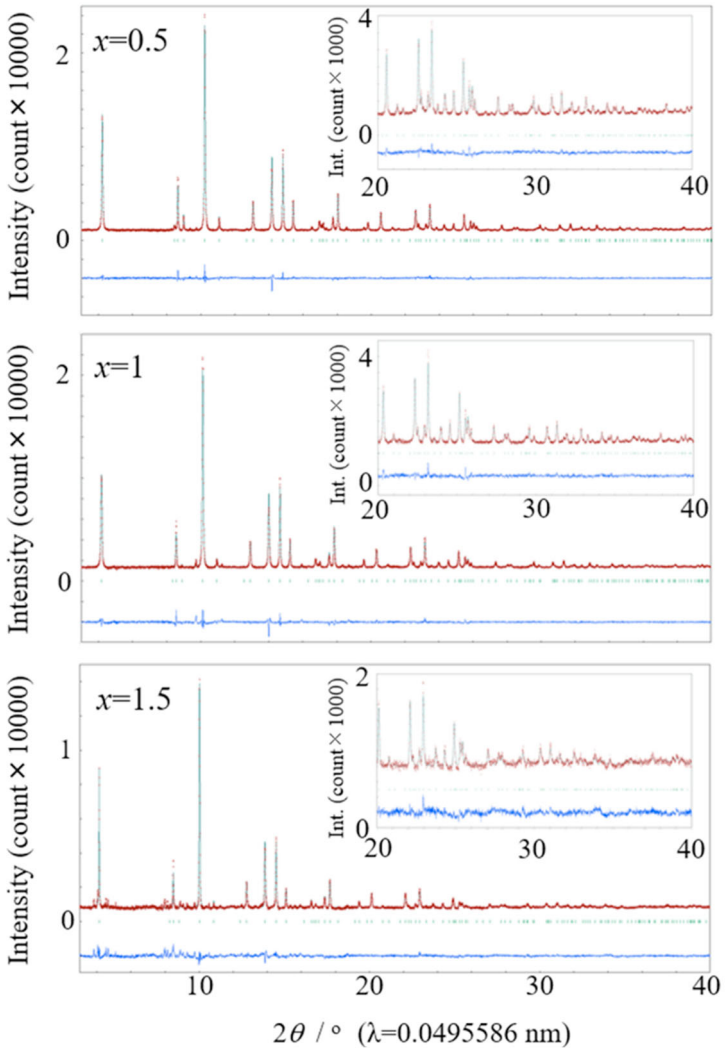

Fig. 3. Rietveld profiles of synchrotron X-ray diffraction patterns of $NaInS_{2-x}Se_x$ measured at 300 K. Green bars represent the allowed reflections for $NaInS_{2-x}Se_x$. Bottom lines give the difference between observed and calculated profiles. Insets show enlargements between 20° and 40°.

Table 1 Refinement and structural summary of NaInS2-xSex measured at 300 K.

x	0	0.5	1	1.5	2
Space Group	R$\bar{3}$m	R$\bar{3}$m	R$\bar{3}$m	R$\bar{3}$m	R$\bar{3}$m
a (nm)	0.3803	0.384123(4)	0.388371(5)	0.392165(10)	0.3972
c (nm)	19.89	2.01608(3)	2.04050(3)	2.06145(7)	2.089
z (S/Se)	0.260	0.25969(6)	0.25987(8)	0.25994(16)	0.26
Na–S/Se (nm)	0.288	0.29044(8)	0.29402(11)	0.2970(3)	0.301
In–S/Se(nm)	0.264	0.26688(7)	0.26972(10)	0.27231(19)	0.276
R_B (%)	–	1.87	2.50	14.07	–
R_F (%)	–	1.27	0.98	5.52	–
R_{WP} (%)	–	3.72	4.07	6.53	–
R_P (%)	–	2.79	4.68	4.52	–
S	–	1.37	1.60	1.98	–
Reference	[8]	this work	this work	this work	[8]

Atomic positions: In(0,0,0), Na(0,0,1/2), S/Se(0,0,z), occupancy of Se in S/Se site is $x/2$ (x = 0.5, 1, 1.5).

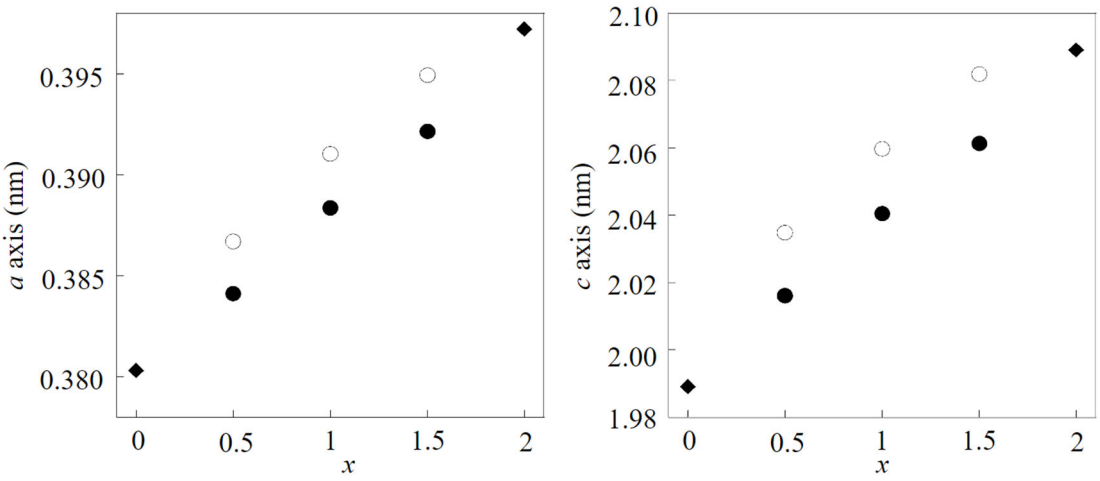

Fig. 4. Lattice parameters of $NaInS_{2-x}Se_x$. The filled and open round marks represent the lattice parameters measured at 300 and 675 K, respectively. The filled diamond marks are reference data [8].

The samples of $NaInS_2$ (x = 0), $NaInS_{1.5}Se_{0.5}$ (x = 0.5), NaInSSe (x = 1), and $NaInS_{0.5}Se_{1.5}$ (x = 1.5) are light grey, yellow, brick-red and ocher, respectively (Fig. 5). The band gap of $NaInS_2$, estimated by linear extrapolation, was 3.32 eV, which is close to previous reports [10, 11]. The band gaps of $NaInS_{2-x}Se_x$ were 2.89 eV for $NaInS_{1.5}Se_{0.5}$ (x = 0.5), 2.31 eV for NaInSSe (x = 1.5), and 2.48 eV for $NaInS_{0.5}Se_{1.5}$ (x = 1.5). Thus, higher Se substitution tends to narrow the band gap of $NaInS_{2-x}Se_x$ although the band gap of NaInSSe (x = 1) was slightly narrower than that of $NaInS_{0.5}Se_{1.5}$ (x = 1.5).

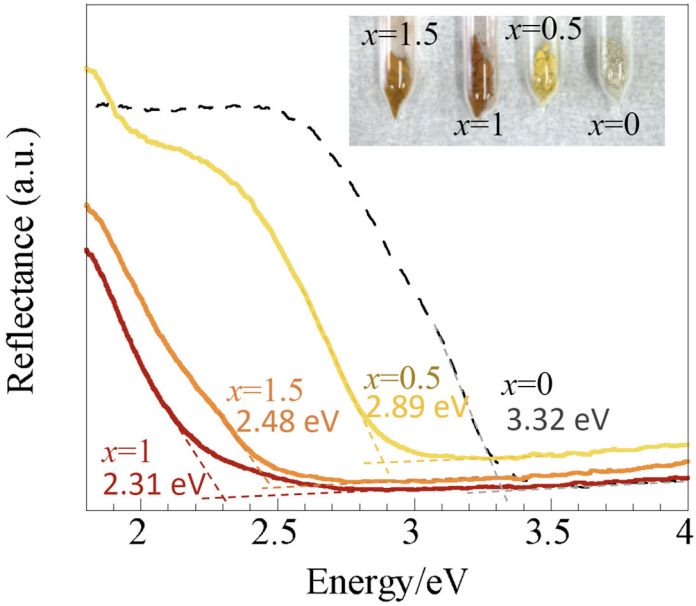

Fig. 5. Optical reflectance and photograph of the $NaInS_{2-x}Se_x$ powders synthesized by ball milling and subsequent heating to 675 K.

The band structures and pDOS of $NaInS_2$ and $NaInSe_2$ have been calculated using the GGA/PBE functional. These results are close to the previous computational results [13, 14]. They were found to be indirect semiconductors. While their valence bands are composed mainly of S/Se, their conduction bands are composed of both In and S/Se. Since the electronic states of Se are higher than those of S, the resulting valence state would form a narrower band gap in $NaInSe_2$ (1.0 eV) than in $NaInS_2$ (1.8 eV); these absolute values are significantly underestimated by the GGA/PBE approach. Thus, the overall trend we observed by Se doping is supported by these calculations. The band structures of $NaInS_2$ and $NaInSe_2$ are calculated to be similar. Nonetheless, even though the difference in energy is less than 0.1 eV, the bottom of

their conduction bands are different: F point ($NaInS_2$) and Γ point ($NaInSe_2$). Thus, the slightly narrower optical band gap of NaInSSe (x = 1) compared to that of $NaInS_{0.5}Se_{1.5}$ (x = 1.5), can be explained by the change in their band structures and/or their defect states.

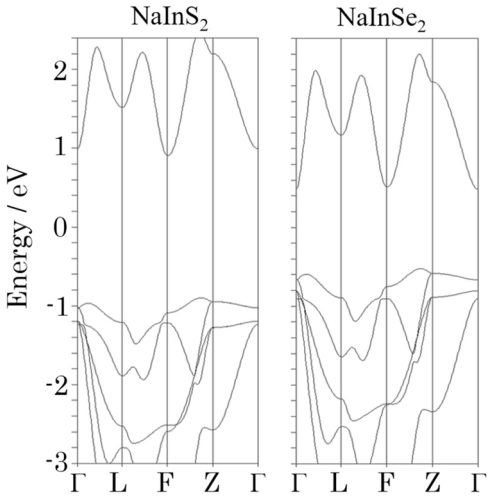

Fig. 6. Band structures of $NaInS_2$ and $NaInSe_2$ predicted by DFT calculation using GGA/PBE functional.

In summary, we confirmed three layered chalcogenides, $NaInS_{1.5}Se_{0.5}$, NaInSSe and $NaInS_{0.5}Se_{1.5}$, by in-situ synchrotron X-ray diffraction techniques. They are layered rock salt structures composed of alternate Na-S/Se and In-S/Se layers. With increasing Se content, their lattice parameters increased and their band gaps tended to decrease. The band gap of NaInSSe was found to be ~2.3 eV. These results demonstrated the usefulness of rapid screening by X-ray diffraction and the potential of $NaInS_{2-x}Se_x$ as optoelectronic materials under visible light exposure.

Acknowledgements

This work was partially supported by JSPS KAKENHI Grant Number 16H04493 and 17H04950. NT was supported by Special Doctoral Program for Green Energy Conversion Science and Technology in University of Yamanashi.

Supporting Information

CIF files of $NaInS_{1.5}Se_{0.5}$, NaInSSe and $NaInS_{0.5}Se_{1.5}$ at 300 and 675 K.

References

[1] J. Voigt, F. Spiegelberg, M. Senoner, Band parameters of CdS and CdSe single crystals determined from optical exciton spectra, physica status solidi (b), 91 (1979) 189-199.

[2] E.A. Axtell, Y. Park, K. Chondroudis, M.G. Kanatzidis, Incorporation of A2Q into HgQ and Dimensional Reduction to $A_2Hg_3Q_4$ and $A_2Hg_6Q_7$ (A = K, Rb, Cs; Q = S, Se). Access of Li Ions in $A_2Hg_6Q_7$ through Topotactic Ion-Exchange, J. Am. Chem. Soc., 120 (1998) 124-136.

[3] R. Banerjee, R. Jayakrishnan, R. Banerjee, P. Ayyub, Effect of the size-induced structural transformation on the band gap in CdS nanoparticles, J. Phys.: Condens. Matter, 12 (2000) 10647.

[4] B.S. Zou, R.B. Little, J.P. Wang, M.A. El-Sayed, Effect of different capping environments on the optical properties of CdS nanoparticles in reverse micelles, Int. J. Quantum Chem, 72 (1999) 439-450.

[5] S. Wagner, J.L. Shay, P. Migliorato, H.M. Kasper, $CuInSe_2$/CdS heterojunction photovoltaic detectors, Appl. Phys. Lett., 25 (1974) 434-435.

[6] A.M. Gabor, J.R. Tuttle, D.S. Albin, M.A. Contreras, R. Noufi, A.M. Hermann, High - efficiency $CuIn_xGa_{1-x}Se_2$ solar cells made from $(In_xGa_{1-x})_2Se_3$ precursor films, Appl. Phys. Lett., 65 (1994) 198-200.

[7] I. Repins, M.A. Contreras, B. Egaas, C. DeHart, J. Scharf, C.L. Perkins, B. To, R. Noufi, 19·9%-efficient ZnO/CdS/$CuInGaSe_2$ solar cell with 81.2% fill factor, Progress in Photovoltaics: Research and Applications, 16 (2008) 235-239.

[8] R. Schneider, Ueber neue Schwefelsalze, Journal für Praktische Chemie, 9 (1874) 209-216.

[9] R. Hoppe, W. Lidecke, F.-C. Frorath, Zur Kenntnis von $NaInS_2$ und $NaInSe_2$, Z. Anorg. Allg. Chem., 309 (1961) 49-54.

[10] K. Fukuzaki, S. Kohiki, S. Matsushima, M. Oku, T. Hideshima, T. Watanabe, S. Takahashi, H. Shimooka, Preparation and characterization of $NaInO_2$ and $NaInS_2$, J. Mater. Chem., 10 (2000) 779-782.

[11] A. Kudo, A. Nagane, I. Tsuji, H. Kato, H_2 Evolution from Aqueous Potassium Sulfite Solutions under Visible Light Irradiation over a Novel Sulfide Photocatalyst $NaInS_2$ with a Layered Structure, Chem. Lett., 31 (2002) 882-883.

[12] R. Saniz, J. Bekaert, B. Partoens, D. Lamoen, Structural and electronic properties of defects at grain boundaries in $CuInSe_2$, PCCP, 19 (2017) 14770-14780 (in supporting information).

[13] K. Persson, Materials Data on $NaInS_2$ (SG:166) by Materials Project, in, 2014.

[14] K. Persson, Materials Data on $NaInSe_2$ (SG:166) by Materials Project, in, 2014.

[15] K. Fukuzaki, S. Kohiki, H. Yoshikawa, S. Fukushima, T. Watanabe, I. Kojima, Changes in the electronic structure of $CuInS_2$ thin films by Na incorporation, Appl. Phys. Lett., 73 (1998) 1385-1387.
[16] L.E. Oikkonen, M.G. Ganchenkova, A.P. Seitsonen, R.M. Nieminen, Effect of sodium incorporation into $CuInSe_2$ from first principles, J. Appl. Phys., 114 (2013) 083503.
[17] P. Hu, C.K. Ngaw, Y.Y. Tay, S. Cao, J. Barber, T.T. Tan, S.C. Loo, A "uniform" heterogeneous photocatalyst: integrated p-n type $CuInS_2/NaInS_2$ nanosheets by partial ion exchange reaction for efficient H_2 evolution, Chem Commun (Camb), 51 (2015) 9381-9384.
[18] Z. Mei, S. Ouyang, D.M. Tang, T. Kako, D. Golberg, J. Ye, An ion-exchange route for the synthesis of hierarchical $In_2S_3/ZnIn_2S_4$ bulk composite and its photocatalytic activity under visible-light irradiation, Dalton Trans, 42 (2013) 2687-2690.
[19] S.E. Creutz, R. Fainblat, Y. Kim, M.C. De Siena, D.R. Gamelin, A Selective Cation Exchange Strategy for the Synthesis of Colloidal $Yb^{(3+)}$-Doped Chalcogenide Nanocrystals with Strong Broadband Visible Absorption and Long-Lived Near-Infrared Emission, J Am Chem Soc, 139 (2017) 11814-11824.
[20] A. Miura, T. Oshima, K. Maeda, Y. Mizuguchi, C. Moriyoshi, Y. Kuroiwa, Y. Meng, X.-D. Wen, M. Nagao, M. Higuchi, K. Tadanaga, Synthesis, structure and photocatalytic activity of layered $LaOInS_2$, Journal of Materials Chemistry A, 5 (2017) 14270-14277.
[21] T. Friscic, I. Halasz, P.J. Beldon, A.M. Belenguer, F. Adams, S.A. Kimber, V. Honkimaki, R.E. Dinnebier, Real-time and in situ monitoring of mechanochemical milling reactions, Nat Chem, 5 (2013) 66-73.
[22] D.P. Shoemaker, Y.-J. Hu, D.Y. Chung, G.J. Halder, P.J. Chupas, L. Soderholm, J.F. Mitchell, M.G. Kanatzidis, In situ studies of a platform for metastable inorganic crystal growth and materials discovery, Proceedings of the National Academy of Sciences, 111 (2014) 10922-10927.
[23] A.J. Martinolich, J.A. Kurzman, J.R. Neilson, Circumventing Diffusion in Kinetically Controlled Solid-State Metathesis Reactions, J Am Chem Soc, 138 (2016) 11031-11037.
[24] S. Kawaguchi, M. Takemoto, K. Osaka, E. Nishibori, C. Moriyoshi, Y. Kubota, Y. Kuroiwa, K. Sugimoto, High-throughput powder diffraction measurement system consisting of multiple MYTHEN detectors at beamline BL02B2 of SPring-8, Rev Sci Instrum, 88 (2017) 085111.
[25] F. Izumi, K. Momma, Three-dimensional visualization in powder diffraction, Solid State Phenom., 130 (2007) 15-20.
[26] K. Momma, F. Izumi, VESTA: a three-dimensional visualization system for electronic and structural analysis, J. Appl. Crystallogr., 41 (2008) 653-658.

[27] G. Kresse, J. Hafner, Ab initio molecular dynamics for liquid metals, Physical Review B, 47 (1993) 558-561.
[28] P.E. Blöchl, Projector augmented-wave method, Physical Review B, 50 (1994) 17953-17979.
[29] G. Kresse, D. Joubert, From ultrasoft pseudopotentials to the projector augmented-wave method, Physical Review B, 59 (1999) 1758-1775.
[30] J.P. Perdew, J.A. Chevary, S.H. Vosko, K.A. Jackson, M.R. Pederson, D.J. Singh, C. Fiolhais, Atoms, molecules, solids, and surfaces: Applications of the generalized gradient approximation for exchange and correlation, Physical Review B, 46 (1992) 6671-6687.